Metal–Organic Frameworks

International Edition: DOI: 10.1002/anie.201504242
German Edition: DOI: 10.1002/ange.201504242

Hollow Zn/Co ZIF Particles Derived from Core–Shell ZIF-67@ZIF-8 as Selective Catalyst for the Semi-Hydrogenation of Acetylene

Jian Yang, Fengjun Zhang, Haiyuan Lu, Xun Hong, Hailong Jiang, Yuen Wu, and Yadong Li**

Abstract: *The rational design of metal–organic frameworks (MOFs) with hollow features and tunable porosity at the nanoscale can enhance their intrinsic properties and stimulates increasing attentions. In this Communication, we demonstrate that methanol can affect the coordination mode of ZIF-67 in the presence of Co^{2+} and induces a mild phase transformation under solvothermal conditions. By applying this transformation process to the ZIF-67@ZIF-8 core–shell structures, a well-defined hollow Zn/Co ZIF rhombic dodecahedron can be obtained. The manufacturing of hollow MOFs enables us to prepare a noble metal@MOF yolk-shell composite with controlled spatial distribution and morphology. The enhanced gas storage and porous confinement that originate from the hollow interior and coating of ZIF-8 confers this unique catalyst with superior activity and selectivity toward the semi-hydrogenation of acetylene.*

To impart new functionalities and properties, enormous efforts have been made to build metal-based composites such as metal/metal and metal/metal oxide composites.[1] Recently, the metal nanoparticles (NPs)@MOFs composite has shown a lot of advantages as a new type of catalyst and thus became a rising star.[2] For example, encapsulation of metal NPs within MOFs can prevent agglomeration and effectively enhance the thermodynamic stability.[3] Organic functional groups of MOFs could serve as Lewis base or acid to implement the metal sites in certain Lewis base-/acid-catalyzed processes.[4] Moreover, the well-defined porous structure of MOFs can confer the shape- or size-selectivity properties if the dimension of reactants and products were carefully modulated.[5] However, when the catalytic process occurs inside the pores, the diffusion control by reactants or products should be taken into account. To this end, the hollow interior of MOFs would facilitate the diffusion of substrates onto the internal metal surface as well as the desorption of products.[6] To date, the construction of hybrid metal@hollow MOFs, simultaneously controlling their composition, morphology, and spatial distribution, are highly desired, but yet challenging.[7]

Zeolite imidazolate frameworks (ZIF) are promising and widely used MOFs for heterogeneous catalysis due to their uniform pore size, well-defined morphology, and excellent chemical stability.[8] The strong coordination between metal ions and imidazolate enables the use of ZIFs in commonly used solvents and the structural integrity can survive even in water which is usually problematic for MOFs. However, the construction of a hollow interior in ZIFs, which will destroy the stable coordination bond, is facing tremendous challenges. Recent efforts in creating ZIF-based hollow or yolk-shell structures used a template such as a polymer or oxides.[9] However, the drastic process for template removal will damage the uniform ordered porous structure and distort the original rhombic dodecahedron morphology. As a consequence, the as-prepared hollow ZIFs usually exhibit a polycrystalline nature and problems like channel plugging occur. Herein, we present a spontaneous phase transformation of ZIF-67 ($[Co(MeIm)_2]_n$) (MeIm = methylimidazole) from a rhombododecahedron to a hollow architecture under mild solvothermal conditions. Given that ZIF-67 and ZIF-8 ($[Zn(MeIm)_2]_n$) are isostructural,[10] a well-defined core–shell ZIF-67@ZIF-8 structure can be generated by epitaxial growth. Further, utilizing the phase transformation of internal ZIF-67, we were able to successfully prepare hollow rhombic dodecahedral Zn/Co ZIF with a regular morphology and single-crystal features. This sequential synthetic strategy empowered the rational design of a multifunctional catalyst with enhanced gas storage and molecular sieving properties.

Employing a cobalt ion as metallic node, 2-methylimidazole as organic linker, and methanol as solvent, the ZIF-67 rhombododecahedron with an average size of 300 nm was synthesized as seeds (Figure 1 a).[11] As shown by transmission electron microscopy (TEM; Figure 1) and scanning electron microscopy (SEM; Figure S1), the parent ZIF-67 would readily evolve into a distinctive hollow nanocage (defined as H-Co-ZIF) after 60 min of solvothermal treatment in methanol. In the first 15 min, some nanoflakes emerged and stacked on the outer surface of solid nanospheres, which was accompanied by a size reduction of the inner core from 300 nm to 250 nm (Figure 1 b). When the process was

[*] H. Lu, X. Hong, Y. Wu, Y. Li
Center of Advanced Nanocatalysis
University of Science and Technology of China (CAN-USTC)
Hefei, Anhui 230026 (P.R. China)
and
Department of Chemistry, Tsinghua University
Beijing 100084 (P.R. China)
E-mail: yuenwu@ustc.edu.cn
ydli@mail.tsinghua.edu.cn
J. Yang,[+] F. Zhang[+]
Center of Advanced Nanocatalysis
University of Science and Technology of China (CAN-USTC)
Anhui Key Laboratory of Advanced Building Materials
Anhui Jianzhu University
Hefei, Anhui 230026 (P.R. China)
H. Jiang
Hefei National Laboratory for Physical Sciences at the Microscale
Department of Chemistry
University of Science and Technology of China
Hefei, Anhui 230026 (P.R. China)
[+] These authors contributed equally to this work.

Supporting information for this article is available on the WWW under http://dx.doi.org/10.1002/anie.201504242.

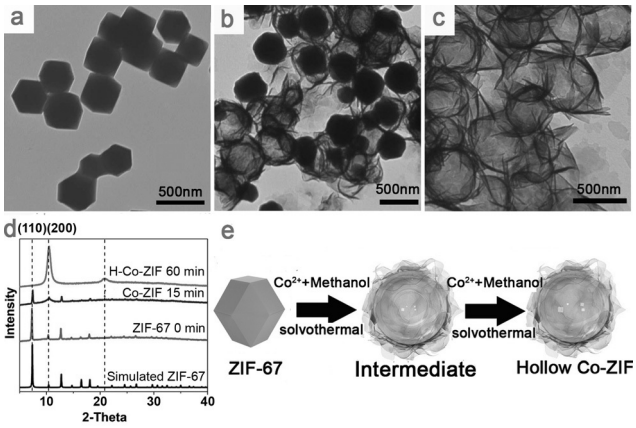

Figure 1. TEM images of a) ZIF-67 rhombododecahedron, b) intermediate, and c) hollow Co-ZIF. d) XRD patterns of ZIF-67 and hollow Co-ZIF. e) Illustration of the structural evolution of ZIF-67.

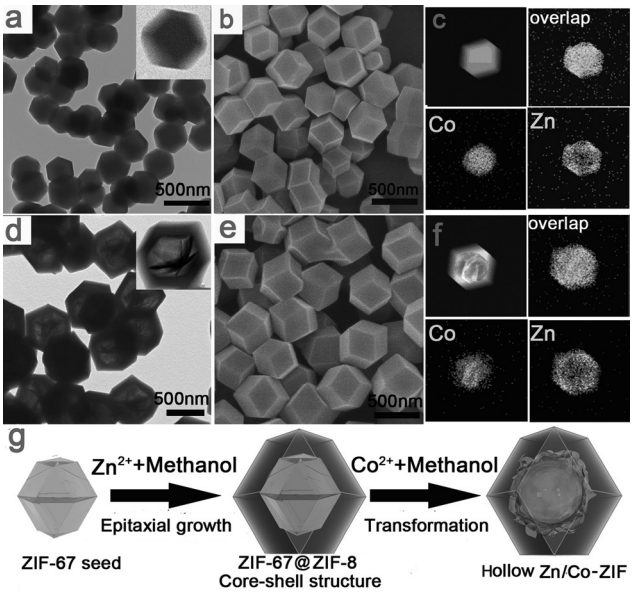

Figure 2. a) TEM image, b) SEM image, and c) EDS mappings of C-Zn/Co-ZIF. d) TEM image, e) SEM image, and f) EDS mappings of H-Zn/Co-ZIF. g) Illustration of the structural evolution.

prolonged to 1 h, it was observed that all of the solid ZIF-67 had transformed to hollow nanocages which were constructed of interlaced flakes (Figure 1c).

X-ray powder diffraction (XRD) was measured to verify the composition and structural evolution (Figure 1d). At the beginning, the peaks of starting seeds matched well with the patterns of simulated ZIF-67. Whereas the characteristic peaks of ZIF-67 ($2-\theta = 7.4°$) readily vanished, two broad peaks ascribed to the gradually formed hollow nanocages emerged at 10.4° and 20.8°, respectively. Unfortunately, the very simple XRD pattern of H-Co-ZIF prevents us to obtain detailed structural information. To further gain insight into the structure of H-Co-ZIF, we performed LC-MS/MS (liquid chromatography tandem mass spectrometry) to get information on the building blocks (Figure S2). According to the fragment signals, it was proposed that methanol molecules may be involved in the unit cell by forming H-bonds in the presence of Co^{2+}. This affects the coordination mode between Co^{2+} and 2-methylimidazole, which would drive the structural evolution from ZIF-67 to H-Co-ZIF. This exchange coincided well with the results obtained by UV/Vis diffuse reflection spectroscopy (Figure S3). The reduced bands at 584 nm and 540 nm, which are characteristic of Co^{2+} in tetrahedral coordination,[12] indicated the evolution of the coordination mode along with the phase transformation. Meanwhile, a color variation from purple to yellow was also observed for a series of samples collected during the evolution from ZIF-67 to H-Co-ZIF.

More importantly, this spontaneous phase transformation can be extended to build hollow ZIF structures. In detail, a uniform ZIF-67@ZIF-8 core–shell structure (defined as C-Zn/Co-ZIF) with a size of 350 nm was firstly generated by sequential nucleation. Under the crystallization conditions, the ZIF-8 favored heterogeneous nucleation in the presence of ZIF-67 seeds due to their isostructural character with similar unit cell and coordination mode. We found that the heterogeneous nucleation still succeeded if the Zn^{2+} and Co^{2+} were introduced both at the beginning of the synthesis. In that case, another solid Zn/Co ZIF (S-Zn/Co-ZIF) owning a homogenous distribution for Zn and Co was obtained (Figure S4). Both the TEM (Figure 2a) and SEM (Figure 2b) images demonstrated that the core–shell structure has well-defined rhombic dodecahedron shape and uniform size (350 nm). The topological feature of the typical core–shell structure was confirmed by the corresponding elementary mapping and line scan (Figures 2c and S5). The distribution of Co and Zn showed that the Co-containing ZIF-67 was located at the interior of the rhombic dodecahedron and encapsulated by the Zn-containing ZIF-8 shell. Then, by treating this core–shell structure with Co^{2+} in methanol at 120 °C for 4 h, the solid interior would readily vanish and form a hollow structure stacked by interlaced nanoplates (Figure S6). According to the SEM, TEM, and HAADF-STEM results, this phase transformation would cause a size enlargement of interior Co-ZIF and thus generate strain at the interface of ZIF-67 core and ZIF-8 shell (Figures S7 and S8). Although the coordination bond between Zn^{2+} and MeIm is stronger than that of Co^{2+}, this strain was enough to excavate the ZIF-8 shell from the inside out. The dissociated Zn^{2+} would diffuse out through the channels and coordinate with the free linkers in solution again. The freshly generated ZIF-8 would deposit on the outside surface of rhombic dodecahedron in this coordination equilibrium. As shown in Figure 2d, the ZIF-8 shell could preserve the initial morphology and symmetry and hold the H-Co-ZIF adjacent to its internal surface, thus forming a unique hollow yolk-shell structure (defined as H-Zn/Co-ZIF). The SEM image (Figure 2e) also evidenced that the integrity of the rhombic dodecahedron shape was not destroyed by the diffusion of metal ions and MeIm through the porous channels. Based on the disparate signals of Zn and Co in elementary mapping (Figure 2f), the core–shell-like spatial distribution was confirmed. That is, the Co^{2+} is concentrated in the core, whereas Zn^{2+} is mainly present in the shell.

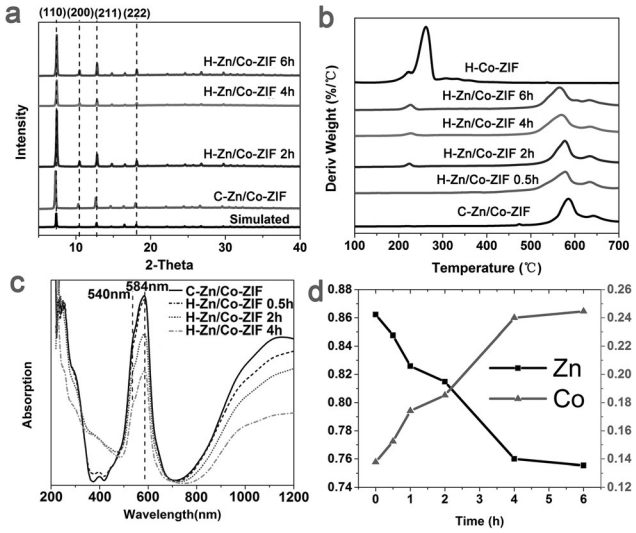

Figure 3. a) XRD, b) TGA, c) UV/Vis diffuse reflection spectrum, and d) ICP-AES measurements tracing the formation of H-Zn/Co-ZIF with different solvothermal reaction time.

Our conclusion as to the phase of the ZIF-8 shell staying unchanged during the formation of H-Zn/Co-ZIF was fully corroborated by the XRD patterns (Figure 3a). The phase of this hetero-ZIF retained the ideal sodalite crystal form, which is mainly attributed to the robustness of the ZIF-8 shell. Although the characteristic XRD peak ($2-\theta = 20.8°$) of H-Co-ZIF was not observed in the XRD patterns due to the hindrance by ZIF-8, the phase transformation of inner ZIF-67 was clearly observed by the measurement of TGA (thermogravimetric analysis). The typical weight loss of H-Co-ZIF was attributed to linker decomposition starting at about 230 °C, which differed with the decomposition of ZIF-8 (600 °C) and ZIF-67 (550 °C) in temperature (Figure S9). This result provides an effective tool to identify the existence of H-Co-ZIF in the hetero Zn/Co ZIFs. A series of samples have been collected in a time-dependent synthesis for further TGA measurements. As shown in Figure 3b, the hetero Zn/Co ZIF obtained after only 2 h solvothermal treatment showed an obvious peak at 230 °C, evidencing the initial formation of the H-Co-ZIF phase.

Similarly, the exchange of coordination mode of interior Co-containing ZIF during the structural transformation from C-Zn/Co-ZIF to H-Zn/Co-ZIF was also reflected by UV/Vis absorption spectra. The same tendency was observed for the band assigned to the tetrahedral Co-MeIm structure[13] and an analogous color evolution was recorded (Figures 3c and S10). The atomic ratio of Zn and Co analyzed by ICP-AES (inductively coupled plasma atomic emission spectrometry; Figure 3d) showed that the concentration of Zn gradually decreased, indicating the etching of the ZIF-8 shell at the internal surface and the integration of isolated Co^{2+} with internal ZIF-67. FTIR spectra of the as-synthesized ZIF-8, ZIF-67, and H-Zn/Co-ZIF were measured to identify the surface functional groups and observe the formation of a coordination polymer (Figure S11). The band at 2929 cm^{-1} attributed to the aliphatic C–H stretch and the band at 584 cm^{-1} assigned to the C≡N stretch mode both showed that 2-methylimidazole is the dominating ligand in these ZIFs. This demonstrated that the linker of 2-methylimidazole remained unchanged during the phase transformation. More importantly, the band at 421 cm^{-1} originating from the Zn–N or Co–N stretch demonstrated that Zn/Co hollow ZIF was a kind of coordination polymer.[10] The elemental valence states of as-prepared H-Zn/Co-ZIF were measured by X-ray photoelectron spectroscopy (XPS). As shown in Figure S12, the spectra of Zn 2p were in good agreement with its oxidation state. The N 1s situated at 406.6 eV was assigned to the MeIm linker. It is worth pointing out that the signal corresponding to Co^{2+} was largely depressed due to the encapsulation of H-Co-ZIF in the ZIF-8 shell. Unlike former reports, which demonstrate that hollow ZIF-8 usually adopted a polycrystalline state, in our case, the presented hollow ZIF-8 retained its crystal orientation, geometrical symmetry, and pore-size distribution during this moderate colloidal method.

We further adopted this hollow H-Zn/Co-ZIF as nanomolds for hosting Pd NPs to evaluate their catalytic performance toward CO oxidation and semi-hydrogenation of acetylene. To construct this metal NPs/MOF nanoreactor, the presynthesized Pd nanoparticles with an average size of 10 nm (Figures S13 and S14) were first loaded on the surface of the ZIF-67 rhombododecahedrons. Then, a sandwich-like structure with Pd NPs situated between the ZIF-67 core and the ZIF-8 shell was obtained by a follow-up encapsulation. Along with the phase transformation of internal ZIF-67, the Pd NPs were successfully placed and confined in the hollow cavities of H-Zn/Co-ZIF. TEM images (Figure 4a) showed that the Pd@H-Zn/Co-ZIF obtained after 4 h solvothermal process were in the form of well-dispersed rhombic dodecahedrons. The high-angle annular dark-field scanning TEM (HAADF-STEM) in Figure 4b as well as the corresponding elementary mapping in Figure 4c both indicated that this composite was composed of hollow coordination polymer and embedded Pd NPs. Compared with solid ZIF, the hollow structure could mitigate the diffusion limitations and thus enhance the catalytic efficiency due to the easier accessibility of substrate to the metal surface. To reinforce our prediction, another composite catalyst of Pd NPs@S-Zn/Co-ZIF was prepared through a coprecipitation process (see details in the Supporting Information, SI). Consistent with the TEM observations (Figure 4d), the corresponding mappings reflected the full encapsulation of the Pd NPs within solid ZIF, in which both Zn and Co are distributed homogeneously (Figure 4d and f). The surface area and pore-size distribution of H-Zn/Co-ZIF and S-Zn/Co-ZIF was analyzed by Brunauer–Emmett–Teller (BET) measurements (Figure S15). Derived from the N_2 adsorption isotherms, the H-Zn/Co-ZIF showed a typical BET surface of 1027 $m^2 g^{-1}$, which was consistent with that of previously reported ZIF-8.[14] Compared with the as-prepared S-Zn/Co-ZIF, the ZIF-8 shell of H-Zn/Co-ZIF with single-crystalline and uniform morphology retained its cavity size and apertures after the phase transformation.

It is worth pointing out two structural superiorities of H-Zn/Co-ZIF in heterogeneous catalysis. On one hand, the hollow interior may enhance gas storage and accelerate desorption of the product. Figure S16 shows the catalytic

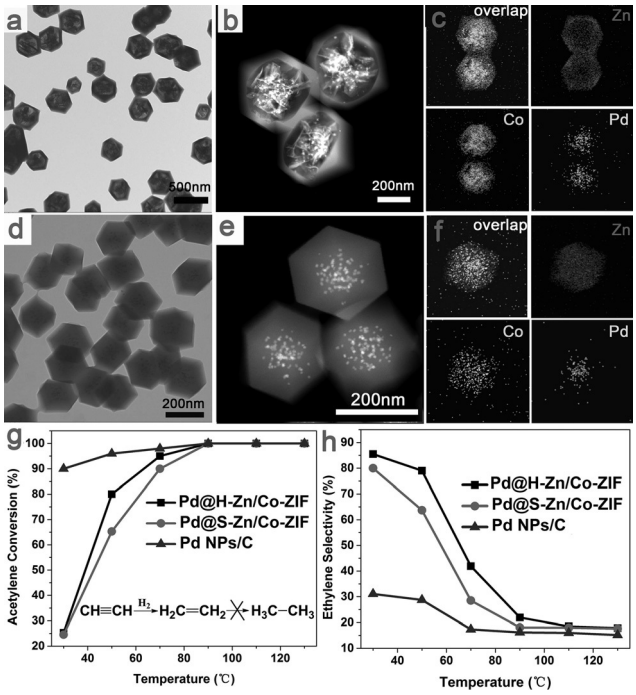

Figure 4. a) TEM pattern, b) HAADF-STEM image, and c) EDX mapping of Pd@H-Zn/Co-ZIF. d) TEM pattern, e) HAADF-STEM image, and f) EDX mapping of Pd@S-Zn/Co-ZIF. g) Acetylene conversion and h) ethylene selectivity as a function of temperature.

behavior of Pd@H-Zn/Co-ZIF and Pd@S-Zn/Co-ZIF in CO oxidation reaction. The plot of CO conversion as a function of reaction temperature showed that the hollow structure catalyzed the complete conversion of CO at a lower temperature compared with the solid structure. It is to say that CO storage was largely enhanced by the hollow interior. On the other hand, the porous confinement introduced by encapsulating ZIF may be a new method of molecular sieving. The catalytic semi-hydrogenation of acetylene, which is usually catalyzed by Pd-based catalysts, is a predominant reaction for manufacturing polyethylene in industry. The decisive goal of the hydrogenation process is to avoid overreduction of ethylene to ethane.[15] This selective hydrogenation of a mixture containing 0.5 vol% C_2H_2, 5 vol% H_2, and 50 vol% C_2H_4 in helium was carried out to probe the catalytic behavior of Pd@H-Zn/Co-ZIF, Pd@S-Zn/Co-ZIF, and Pd nanocubes supported on active carbon. Assuming that ethylene is the only product, the selectivity for hydrogenation of acetylene can be well defined and calculated[16] (see details in SI). Figure 4g shows the conversion of acetylene as a function of temperature ranging from 30 °C to 130 °C. In the case of bare Pd NPs/C, high conversion (>90%) of acetylene but low ethylene selectivity (<30%) was achieved at any given temperature. This could be ascribed to the unselective absorption of acetylene and ethylene on the highly exposed Pd surface, resulting in the easy formation of the ethane byproduct. In comparison, for Pd NPs embedded in ZIF, a significant enhancement of ethylene selectivity was observed at 50 °C, although accompanied by a lower conversion. We therefore speculated that the smaller acetylene was more prone to diffuse to the internal Pd NPs than ethylene and thereby facilitates the selective hydrogenation. Further, the Pd@H-Zn/Co-ZIF showed improved activity (>80% conversion of acetylene) and ethylene selectivity (still >80%) relative to Pd@S-Zn/Co-ZIF. The hollow interior of H-Zn/Co-ZIF may enable the increased inward diffusion rate of acetylene and the preferential desorption of ethylene from the Pd surface, which would be a benefit for the efficient and selective semi-hydrogenation of acetylene. Moreover, this composite exhibited excellent catalytic stability during a 10 h on-stream reaction experiments. That is, no obvious decay in conversion of acetylene and ethylene selectivity was observed (Figure S17).

In conclusion, we have demonstrated an effective strategy to construct hollow ZIF-8 structures under mild wet conditions. This strategy is based on the spontaneous phase transformation of ZIF-67 under solvothermal conditions and enables the encapsulation of Pd NPs within the cavities of ZIF-8. The as-prepared Pd@H-Zn/Co-ZIF nanoreactor encompasses the advantages in remitting the diffusion limitation and porous confinement toward some important reactions, which is characterized by the hollow features of ZIF. Our findings may present novel design criteria for advanced metal NPs/MOF nanoscale composites with tunable structure and improved functionalities.

Acknowledgements

This work was supported by the Fundamental Research Funds for the Central Universities (WK2060190043), and the National Natural Science Foundation of China (U1463202).

Keywords: core–shell particles · metal–organic frameworks · semi-hydrogenation of acetylene · zeolite imidazolate frameworks

How to cite: *Angew. Chem. Int. Ed.* **2015**, *54*, 10889–10893
Angew. Chem. **2015**, *127*, 11039–11043

[1] a) B. Wu, N. Zheng, *Nano Today* **2013**, *8*, 168–197; b) Y. Wu, D. Wang, X. Chen, G. Zhou, R. Yu, Y. Li, *J. Am. Chem. Soc.* **2013**, *135*, 12220–12223; c) N. Liu, Y. Yao, J. J. Cha, M. T. McDowell, Y. Han, Y. Cui, *Nano Res.* **2012**, *5*, 109–116.
[2] a) G. Lu, S. Li, Z. Guo, O. K. Farha, B. G. Hauser, X. Qi, Y. Wang, X. Wang, S. Han, X. Liu, *Nat. Chem.* **2012**, *4*, 310–316; b) H. R. Moon, D.-W. Lim, M. P. Suh, *Chem. Soc. Rev.* **2013**, *42*, 1807–1824.
[3] a) H. Khajavi, H. A. Stil, H. P. Kuipers, J. Gascon, F. Kapteijn, *ACS Catal.* **2013**, *3*, 2617–2626; b) C. Hou, G. Zhao, Y. Ji, Z. Niu, D. Wang, Y. Li, *Nano Res.* **2014**, *7*, 1364–1369.
[4] A. Corma, H. Garcia, F. Llabrés i Xamena, *Chem. Rev.* **2010**, *110*, 4606–4655.
[5] J. Lee, O. K. Farha, J. Roberts, K. A. Scheidt, S. T. Nguyen, J. T. Hupp, *Chem. Soc. Rev.* **2009**, *38*, 1450–1459.
[6] Z. Zhang, Y. Chen, S. He, J. Zhang, X. Xu, Y. Yang, F. Nosheen, F. Saleem, W. He, X. Wang, *Angew. Chem. Int. Ed.* **2014**, *53*, 12517–12521; *Angew. Chem.* **2014**, *126*, 12725–12729.
[7] Z. Zhang, Y. Chen, X. Xu, J. Zhang, G. Xiang, W. He, X. Wang, *Angew. Chem. Int. Ed.* **2014**, *53*, 429–433; *Angew. Chem.* **2014**, *126*, 439–443.

[8] a) K. S. Park, Z. Ni, A. P. Côté, J. Y. Choi, R. Huang, F. J. Uribe-Romo, H. K. Chae, M. O'Keeffe, O. M. Yaghi, *Proc. Natl. Acad. Sci. USA* **2006**, *103*, 10186; b) X. C. Huang, Y. Y. Lin, J. P. Zhang, X. M. Chen, *Angew. Chem. Int. Ed.* **2006**, *45*, 1557; *Angew. Chem.* **2006**, *118*, 1587; c) R. Banerjee, A. Phan, B. Wang, C. Knobler, H. Furukawa, M. O'Keeffe, O. M. Yaghi, *Science* **2008**, *319*, 939.

[9] a) C.-H. Kuo, Y. Tang, L.-Y. Chou, B. T. Sneed, C. N. Brodsky, Z. Zhao, C.-K. Tsung, *J. Am. Chem. Soc.* **2012**, *134*, 14345 – 14348; b) F. Zhang, Y. Wei, X. Wu, H. Jiang, W. Wang, H. Li, *J. Am. Chem. Soc.* **2014**, *136*, 13963 – 13966; c) H. J. Lee, W. Cho, M. Oh, *Chem. Commun.* **2012**, *48*, 221 – 223.

[10] J. Tang, R. R. Salunkhe, J. Liu, N. L. Torad, M. Imura, S. Furukawa, Y. Yamauchi, *J. Am. Chem. Soc.* **2015**, *137*, 1572.

[11] J. Qian, F. Sun, L. Qin, *Mater. Lett.* **2012**, *82*, 220 – 223.

[12] M. He, J. Yao, Q. Liu, K. Wang, F. Chen, H. Wang, *Microporous Mesoporous Mater.* **2014**, *184*, 55 – 60.

[13] J. Zakzeski, A. Dębczak, P. C. Bruijnincx, B. M. Weckhuysen, *Appl. Catal. A* **2011**, *394*, 79 – 85.

[14] a) J.-P. Zhang, X.-M. Chen, *J. Am. Chem. Soc.* **2008**, *130*, 6010 – 6017; b) H.-L. Jiang, B. Liu, T. Akita, M. Haruta, H. Sakurai, Q. Xu, *J. Am. Chem. Soc.* **2009**, *131*, 11302 – 11303; c) M. Fang, C. Wu, Z. Yang, T. Wang, Y. Xia, J. Li, *J. Membr. Sci.* **2015**, *474*, 103 – 113.

[15] a) J. Osswald, K. Kovnir, M. Armbrüster, R. Giedigkeit, R. E. Jentoft, U. Wild, Y. Grin, R. Schlögl, *J. Catal.* **2008**, *258*, 219 – 227; b) W. Huang, J. R. McCormick, R. F. Lobo, J. G. Chen, *J. Catal.* **2007**, *246*, 40 – 51.

[16] M. Armbrüster, K. Kovnir, M. Friedrich, D. Teschner, G. Wowsnick, M. Hahne, P. Gille, L. Szentmiklósi, M. Feuerbacher, M. Heggen, *Nat. Mater.* **2012**, *11*, 690 – 693.

Received: May 9, 2015
Revised: July 11, 2015
Published online: August 5, 2015

